Electrical, optical, and structural properties of indium–tin–oxide thin films for organic light-emitting devices

H. Kim[a] and C. M. Gilmore
School of Engineering and Applied Science, George Washington University, 725 23rd Street Northwest, Washington DC 20052

A. Piqué, J. S. Horwitz, H. Mattoussi, H. Murata, Z. H. Kafafi, and D. B. Chrisey
Naval Research Laboratory, 4555 Overlook Avenue Southwest, Washington DC 20375

(Received 15 June 1999; accepted for publication 27 August 1999)

High-quality indium–tin–oxide (ITO) thin films (200–850 nm) have been grown by pulsed laser deposition (PLD) on glass substrates without a postdeposition annealing treatment. The structural, electrical, and optical properties of these films have been investigated as a function of target composition, substrate deposition temperature, background gas pressure, and film thickness. Films were deposited from various target compositions ranging from 0 to 15 wt % of SnO_2 content. The optimum target composition for high conductivity was 5 wt % SnO_2 + 95 wt % In_2O_3. Films were deposited at substrate temperatures ranging from room temperature to 300 °C in O_2 partial pressures ranging from 1 to 100 mTorr. Films were deposited using a KrF excimer laser (248 nm, 30 ns full width at half maximum) at a fluence of 2 J/cm^2. For a 150-nm-thick ITO film grown at room temperature in an oxygen pressure of 10 mTorr, the resistivity was 4×10^{-4} Ω cm and the average transmission in the visible range (400–700 nm) was 85%. For a 170-nm-thick ITO film deposited at 300 °C in 10 mTorr of oxygen, the resistivity was 2×10^{-4} Ω cm and the average transmission in the visible range was 92%. The Hall mobility and carrier density for a 150-nm-thick film deposited at 300 °C were 27 cm^2/V s and 1.4×10^{21} cm^{-3}, respectively. A reduction in the refractive index for ITO films can be achieved by raising the electron density in the films, which can be obtained by increasing the concentration of Sn dopants in the targets and/or increasing deposition temperature. Atomic force microscopy measurements of these ITO films indicated that their root-mean-square surface roughness (~5 Å) was superior to that of commercially available sputter deposited ITO films (~40 Å). The PLD ITO films were used to fabricate organic light-emitting diodes. From these structures the electroluminescence was measured and an external quantum efficiency of 1.5% was calculated. © *1999 American Institute of Physics.* [S0021-8979(99)04223-1]

I. INTRODUCTION

Indium–tin–oxide (ITO) thin films have been studied extensively in the optoelectronic industry because they combine unique transparent and conducting properties. ITO thin film is a highly degenerate *n*-type semiconductor which has a low electrical resistivity of $2-4\times10^{-4}$ Ω cm. The low resistivity value of ITO films is due to a high carrier concentration because the Fermi level (E_F) is located above the conduction level (E_C). The degeneracy is caused by both oxygen vacancies and substitutional tin dopants created during film deposition. The carrier concentration of high conductivity ITO films is in the range of $10^{20}-10^{21}$ cm^3.[1] Furthermore, ITO is a wide band gap semiconductor (E_g: 3.5–4.3 eV), which shows high transmission in the visible and near-IR regions of the electromagnetic spectrum. Due to these unique properties, ITO has been used in a wide range of applications. For example, ITO films are used as transparent electrodes in flat panel displays and solar cells, surface heaters for automobile windows, camera lenses and mirrors as well as transparent heat reflecting window material for buildings, lamps, and solar collectors.[1]

Since ITO films have shown good efficiency for hole injection into organic materials, they have also been widely utilized as the anode contact in organic light-emitting diodes (OLEDs).[2,3] There are several deposition techniques used to grow ITO thin films including chemical vapor deposition (CVD),[4] magnetron sputtering,[5,6] evaporation,[7] and spray pyrolysis.[8] However, these techniques require either a high substrate temperature (300–500 °C) during deposition or a postdeposition annealing treatment of the films at high temperature (400–700 °C). These high temperature treatments generally damage surfaces of both the substrate and the film.

Recently, ITO films have also been grown by pulsed laser deposition (PLD).[2,9–11] PLD provides several advantages compared to other techniques. The composition of films grown by PLD is quite close to that of the target, even for a multicomponent target. PLD films may crystallize at lower substrate temperatures relative to other physical vapor deposition (PVD) techniques due to the high kinetic energies (>1 eV) of the ionized and ejected species in the laser-produced plasma.[12] Also, the surface of films grown by PLD is very smooth, so that ITO films grown by PLD can be used as an anode contact in OLEDs.[2]

In this article, we report a study of the electrical, optical, and structural properties of ITO films deposited by PLD on

[a]Electronic mail: hskim@ccf.nrl.navy.mil

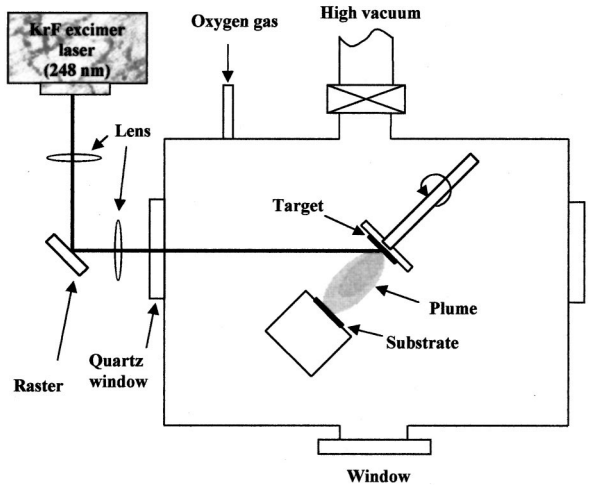

FIG. 1. A schematic diagram of the experimental setup.

glass substrates without a postdeposition anneal. Film properties were measured as a function of target composition, substrate deposition temperature, background gas pressure, and film thickness. Along with this, we present data on the performance of OLEDs using these films as their anode contact.

II. EXPERIMENT

ITO thin films were deposited on glass (microslide glass) substrates using PLD.[12] A schematic diagram of the experimental setup is shown in Fig. 1. A KrF excimer laser (Lambda Physics LPX 305) with a wavelength of 248 nm and pulse duration of 30 ns delivered an energy of 300 mJ per pulse. The laser was operated at 10 Hz and was focused through a 50 cm focal length lens onto a rotating target at a 45° angle of incidence. The energy density of the laser beam at the target surface was maintained at 2 J/cm^2. The target-substrate distance was 4.7 cm. The geometry of this PLD system produced uniform films over 1.5 cm×1.5 cm substrate area with a thickness variation of less than 10%. The substrate was attached with a stainless steel mask to a substrate holder, which was heated by two quartz lamps. The substrate temperature was monitored with a thermocouple at all times.

The ITO targets were prepared from In_2O_3 (purity, 99.999%) and SnO_2 (purity, 99.999%) powders [Alfa AESAR]. The powders were mixed in a mechanical shaker for 1 h, pressed into a 1-in.-diam pellet at 15 000 lb., and then sintered at 1300 °C for 6 h in air. The substrates were cleaned in an ultrasonic cleaner for 10 min with acetone and then methanol. All substrates were blown dry with dry nitrogen gas before they were introduced into the deposition system. During deposition, oxygen background gas was introduced into the chamber to maintain the desired pressure and its pressure was monitored with a MKS pressure/flow controller (type 250 C) from 0.1 to 100 mTorr. Moreover, during deposition, the substrate temperature was fixed to the desired temperature (25–300 °C). After deposition, for films deposited at elevated temperature, the films were cooled to room temperature at the same oxygen pressure. The oxygen pressure and substrate temperature were optimized to obtain high quality films of low resistivity and high transparency.

The film thickness was measured by a stylus profilometer [Tencor Alpha-Step 250]. The sheet resistance (R_s) measurements were performed using a four-point probe. By assuming that the thickness of the films was uniform, the film resistivity (ρ) was determined using the simple relation $\rho = R_s \cdot t$, where t is the film thickness. All sheet resistance and resistivity values were determined as the average of three measurements for each film. Hall mobility and carrier density measurements were made using the van der Pauw method[13] at room temperature with a field strength (B) of 5 kG. The Hall coefficient (R_H) was measured using the formula, $R_H=(10.0Vt)/(IB)$, where V is the average transverse voltage in [mV], I is the dc current in [mA], and t is the thickness of the film in [μm]. The measured Hall coefficient (R_H) was used to calculate the free-electron density (N) of the films by the equation, $N=1/(R_H \cdot e)$, where e is the electron charge. The measured Hall coefficient (R_H) was also used to determine the Hall mobility (μ_H) using the following relation: $\mu_H = R_H \sigma$, where σ is the conductivity. The optical transmission and reflectance measurements were made using an UV-visible–near-IR spectrophotometer [Perkin–Elmer Lambda 9]. Refractive indices of the films were determined from the reflectance maxima data using the following relation: $n \cdot d = k \cdot \lambda/4$, where n is the refractive index, d is the film thickness [nm], λ is the wavelength [nm], and k is the interference order (an odd integer).[14] X-ray diffraction (XRD) [Rigaku rotating anode x-ray generator with Cu $K\alpha$ radiation] was used to characterize the crystal structure of the films. From an analysis of the diffraction pattern, we determined the lattice parameter, preferred orientation, and average grain size of the deposited films. The true peak width (B_s) corresponding to monochromatic x rays was determined by measuring x-ray peak widths and the peak positions, which were analyzed using a peakfit routine with a Gaussian distribution function. The instrumental broadening (B_0) was determined by measuring the diffraction peak width of silicon powder. The corrected peak width (B) can be calculated by the formula $B^2 = B_s^2 - B_0^2$. The calculated peak width (B) was used to determine the grain size (t) using the formula, $t = 0.9\lambda/(B \cos\theta)$, where λ is the x-ray wavelength and θ is the Bragg diffraction angle.[15] X-ray photoelectron spectroscopy (XPS) [VG Scientific, 220I] was used to analyze the film composition. Scanning electron microscopy (SEM) [LEO-1500] and atomic force microscopy (AFM) [Digital Instrument, Dimension 3100 series] were used to evaluate the surface morphology of the films.

III. RESULTS AND DISCUSSION

A. Electrical properties

The electrical properties of ITO films depend on the film composition and deposition parameters such as substrate deposition temperature, oxygen pressure, and film thickness. Figure 2 shows the typical variation of film resistivity (ρ), carrier density (N), and Hall mobility (μ) as a function of the SnO_2 content in the ITO target. The SnO_2 content was varied in the range from 0 to 15 wt %. In our previous study,[2] the

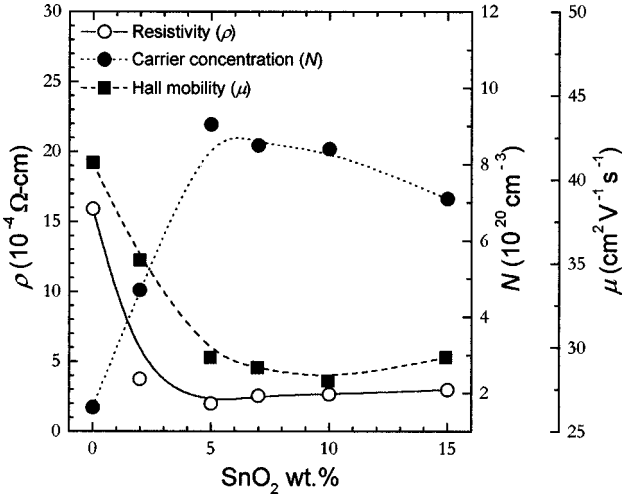

FIG. 2. Dependence of resistivity, carrier density, and Hall mobility on SnO_2 content for the deposited ITO films. The substrate deposition temperature was kept at 250 °C and the oxygen pressure was 10 mTorr during deposition.

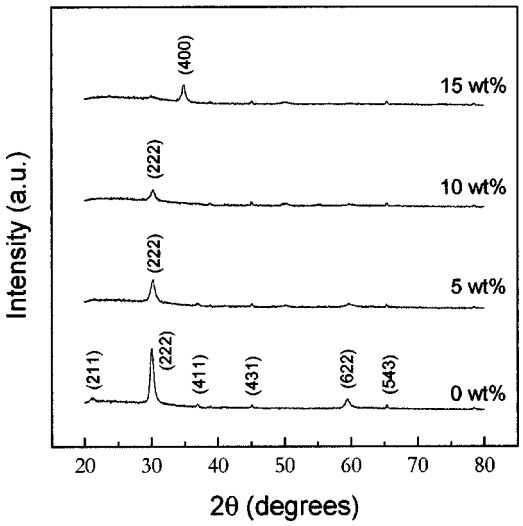

FIG. 3. X-ray diffraction patterns for ITO films deposited on glass from targets with different SnO_2 contents. All films were deposited at 250 °C in 10 mTorr of oxygen.

optimal deposition conditions (substrate deposition temperature and oxygen pressure) for obtaining high conductivity of ITO films were 250 °C and 10 mTorr. Hence, the above optimal deposition conditions were used in this research. In the case of the undoped In_2O_3 film, the carrier density and resistivity were 1.5×10^{20} cm^{-3} and 1.6×10^{-3} Ω cm, respectively. The resistivity of the ITO films was observed to initially decrease with increasing SnO_2 content up to 5 wt %. It was also observed that the carrier density increased with increasing SnO_2 content up to 5 wt %. This initial increase in carrier density resulted in a decrease in the resistivity as a result of the donor electrons from the Sn dopant.[16,17] However, the resistivity of the films, after reaching a minimum (at 5 wt % of SnO_2), gradually increased with a further increase in the SnO_2 content up to 15 wt %. This is due to an increase in the concentration of the electron traps as a result of excess Sn doping. Above the critical Sn content (corresponding to about 5 wt % of SnO_2 content), excess Sn atoms may occupy interstitial positions and some Sn atoms may also form defects such as Sn_2O, Sn_2O_4, and SnO, which act as carrier traps rather than electron donors.[1] The decrease in carrier density and increase in resistivity beyond 5 wt % of SnO_2 content is due to increased disorder of the crystal lattice, which causes phonon scattering and ionized impurity scattering and results in a decrease in mobility.[18] The Sn ion, which is surrounded only by In_2O_3, can behave as a donor. In an over doped state, however, the Sn ion is affected by a second Sn ion due to excess Sn and the interaction of Sn ions leads to a suppression in their donor ability.[19] This result is also correlated with the loss of crystallinity in ITO films for higher dopant levels[17,20] (Fig. 3). Manifacier[16] also suggested that for the ITO films with higher doping levels, the increase in resistivity is due to an increase in disorder, which decreases the mobility and free carrier density. This is in agreement with our results shown in Fig. 2. It was further seen from Fig. 2 that Hall mobility decreased with increasing SnO_2. The decrease in mobility with increase in Sn dopant level was caused by ionized impurity scattering. The optimum SnO_2 content in the ITO target (for minimum film resistivity) was 5 wt %. XPS measurements indicated that the Sn/In ratio (~0.048) of ITO films is similar to that (~0.050) of the target. Hereafter, the 5 wt % SnO_2-doped In_2O_3 target was used to deposit the ITO films described in this work.

The deposition temperature was found to affect the electrical properties of the ITO films. Figure 4 shows the variation of resistivity (ρ), carrier density (N), and Hall mobility (μ), as a function of deposition temperature for the ITO films deposited in an oxygen pressure of 10 mTorr. The resistivity of the ITO films decreased from 3.8×10^{-4} to 1.9×10^{-4} Ω cm as the deposition temperature was increased from 25 to 300 °C. The carrier concentration in the ITO films was observed to gradually increase as the substrate deposition temperature was increased. This increase in carrier concentration may be due to an increase in diffusion of Sn atoms from

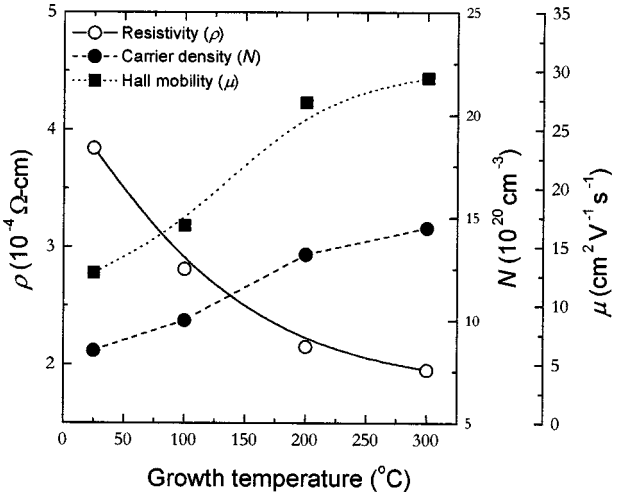

FIG. 4. Variation of resistivity, carrier density, and Hall mobility as a function of substrate deposition temperature for the ITO films deposited in 10 mTorr of oxygen. The target composition used in these experiments was 5 wt % SnO_2+95 wt % In_2O_3. The film thickness was ~200 nm for all films.

TABLE I. Variation of calculated grain size and lattice parameter for the ITO films grown at different deposition temperatures. All films were deposited in 10 mTorr of oxygen using the target with 5 wt % of SnO_2.

Growth temperature (°C)	Film thickness (nm)	Grain size (nm)	Lattice parameter (Å)
25	270±15.5	···	···
100	310±14.1	10	10.2217±0.0072
200	290±12.8	14	10.2251±0.0077
300	300±12.0	20	10.2381±0.0082

interstitial locations and grain boundaries into the In cation sites. Since the Sn atom has a valency of 4 and In is trivalent, the Sn atoms act as donors in ITO films. Hence, the increase in diffusion with the substrate temperature results in higher electron concentration. The decrease in resistivity with increase in deposition temperature can be also explained by the fact that the crystallite size increases[8] significantly with increasing the deposition temperature (see Table I), thus reducing the grain boundary scattering and increasing conductivity (see Fig. 5). This decrease in resistivity was also associated with the observed increase in carrier mobility as shown in Fig. 4. For the films grown at higher deposition temperature (>300 °C), the resistivity was found to increase again. This increase may be due to contamination of the films by alkali ions from glass substrates[13,15,20] and/or by a change in the Sn/In and O/In ratios.[22,23]

The oxygen pressure was also found to affect the electrical properties of the ITO films. Figure 6 illustrates the variation of resistivity (ρ), carrier density (N), and Hall mobility (μ) as a function of oxygen pressure for the ITO films grown at a deposition temperature of 300 °C. It is found that the resistivity of the films remains high $\sim 1.8\times10^{-3}\ \Omega$ cm for oxygen pressures from 50 to 100 mTorr and decreases with decreasing the oxygen pressure from 50 to 10 mTorr. This decrease in resistivity with decrease in oxygen pressure can be explained by the number of oxygen vacancies in the ITO film. The oxygen vacancies create free electrons in the films because one oxygen vacancy creates two extra electrons in the film. The increase in the number of oxygen vacancies leads to an increase in carrier density and a consequent increase in conductivity. This relationship is well illustrated in Fig. 6. The carrier density of the ITO films increases from 2×10^{20} to 11×10^{20} cm^{-3} due to an increase in the number of oxygen vacancies when the oxygen deposition pressure is decreased from 50 to 10 mTorr. Hence, the resistivity of the ITO films decreases with decreasing oxygen pressure from 50 to 10 mTorr due to an increase in the number of oxygen vacancies. However, the resistivity of the ITO films increased with a further decrease in the oxygen pressure (<10 mTorr). This increase in resistivity may be due to the fact that severe oxygen deficiencies may deteriorate the crystalline properties (see Fig. 7) and consequently reduce the mobility of carriers (see Fig. 6). This result is similar to the previous report on the sputtered ITO films.[24] Since the oxygen vacancies were reduced with increasing oxygen pressure, the decrease in carrier density with increasing oxygen pressure suggests that the carrier density resulted from oxygen vacancies as well as tin doping.

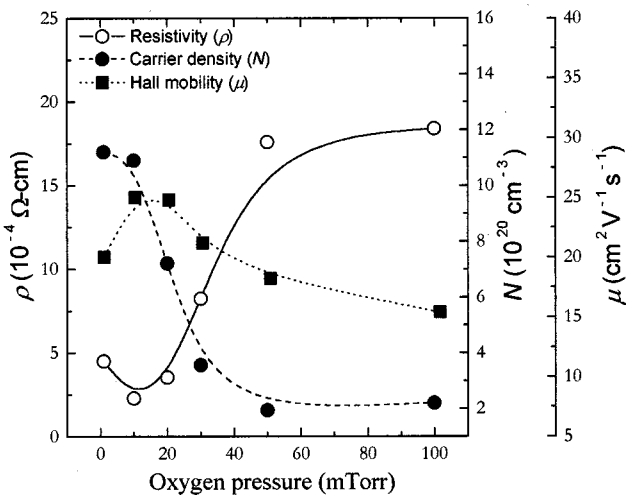

FIG. 6. Variation of resistivity, carrier density, and Hall mobility as a function of oxygen deposition pressure for the films grown at 300 °C. The film thickness was ~200 nm for all films.

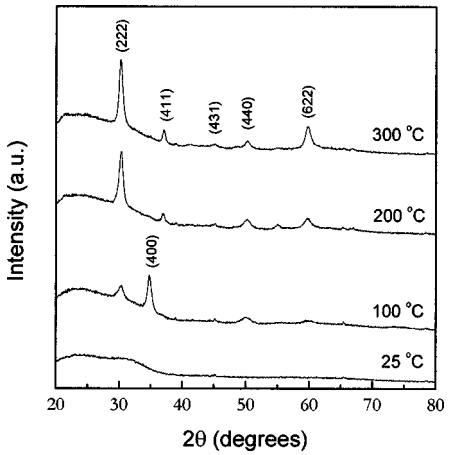

FIG. 5. X-ray diffraction patterns for ITO films grown on glass at different substrate deposition temperatures. The oxygen pressure was kept in 10 mTorr during deposition. The film thickness was ~300 nm for all films.

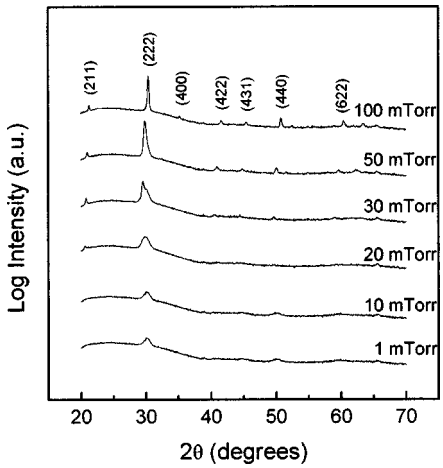

FIG. 7. X-ray diffraction patterns for the ITO films grown on glass at different oxygen pressures. Substrate deposition temperature was 300 °C. The film thickness was ~200 nm for all films.

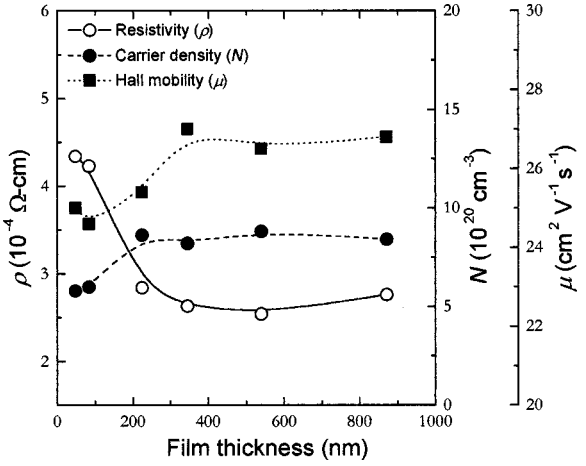

FIG. 8. Variation of resistivity, carrier density, and Hall mobility as a function of film thickness for the films grown at 300 °C and 10 mTorr of oxygen.

Figure 8 shows the effect of the film thickness on the resistivity (ρ), carrier density (N), and Hall mobility (μ) of the ITO films. All the films shown here were grown from the 5 wt % SnO_2-doped In_2O_3 target at the deposition temperature of 300 °C and the oxygen pressure of 10 mTorr. The film thickness is directly proportional to the number of laser shots with an average deposition rate of ~1 Å/shot. As seen in Fig. 8, the resistivity of the ITO films initially decreases with an increase in the film thickness up to 220 nm and remains almost constant with further increase in the film thickness up to 870 nm. It is also observed that the carrier density increases with an increase in the film thickness up to 220 nm and then remains almost constant with further increases in the film thickness up to 870 nm. It is also seen in Fig. 8 that the Hall mobility increases with increasing film thickness. XRD measurements indicate that the thicker films are more crystalline and have larger grains than the thinner films have; the 220-nm-thick film has an average grain size of 20 nm and the 870-nm-thick film has an average grain size of 26 nm. The larger grain size can cause a decrease in grain boundary scattering, which leads to an increase in the conductivity. Thus, the initial decrease in resistivity is due to an increase in both carrier density and carrier mobility of the films. For thicker films (>300 nm), the resistivity remains constant because both carrier density and carrier mobility become independent of film thickness.

B. Optical properties

The optical transmission (T) and reflectance (R) measurements were performed using a UV-VIS-NIR spectrophotometer (Perkin–Elmer Lambda 9) in a two-beam configuration. The transmission and reflectance data were used to calculate absorption coefficients of the ITO films at different wavelengths. The absorption coefficient, α, is given by the relation

$$T=(1-R)\exp(-\alpha d), \tag{1}$$

where d is the film thickness. The absorption coefficient data were used to determine energy gap, E_g, using the relation[25]

$$\alpha h\nu \approx (h\nu - E_g)^{1/2}, \tag{2}$$

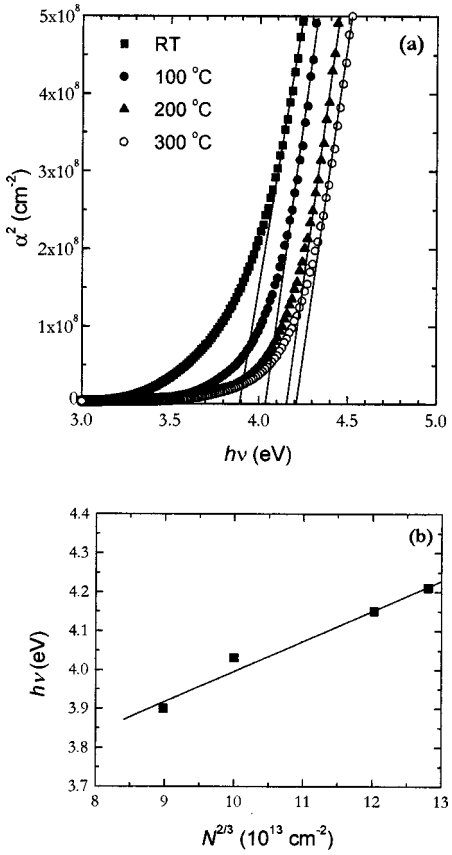

FIG. 9. (a) Dependence of photon energy on α^2 for ITO films grown at different substrate temperatures. (b) Variation of band gap as a function of $N^{2/3}$ for the same films shown in (a).

where $h\nu$ is the photon energy. Figure 9(a) shows α^2 versus a plot of photon energy ($h\nu$) curves for ITO films grown at different temperatures. The values of the direct optical band gap E_g were determined by extrapolations of the linear regions of the plots to zero absorption ($\alpha h\nu = 0$). It was observed that the direct band gap of the ITO films increased from 3.89 to 4.21 eV with an increase in deposition temperature from 25 to 300 °C. This increase in band gap is due to increase in carrier concentration of the films (see Fig. 4). This shift of the band gap with change in carrier concentration can be explained by the Burstein–Moss (B–M) shift.[26,27] Assuming that both the conduction band and valence band are parabolic [Fermi wave number $(k) \propto E^{1/2}$] and the B–M shift is the predominant effect, the band gap, which is the energy gap between the top of the valence band and the lowest empty state in the conduction band can be given by

$$E_g = E_{g0} + \Delta E_g^{\mathrm{B-M}}, \tag{3}$$

where E_{g0} is the intrinsic band gap (~3.75 eV)[28] and $\Delta E_g^{\mathrm{B-M}}$ is the B–M shift, which is the increase due to filling up of low lying energy levels in the conduction band. The B–M shift $\Delta E_g^{\mathrm{B-M}}$ is given by

$$\Delta E_g^{\mathrm{B-M}} = (\hbar^2/2m_{VC}^*)(3\pi^2 N)^{2/3}, \tag{4}$$

where m_{VC}^* is the reduced effective mass of the electron carriers given by

TABLE II. Optical properties of the ITO films grown at 250 °C and 10 mTorr of oxygen as a function of SnO_2 content (wt %). The film thickness was determined by a stylus profilometer and the carrier density was determined from the measured Hall coefficients.

SnO_2 content (wt %)	Film thickness (nm)	Mean transmission (%)	Refractive index at 550 nm	Band gap (eV)	Plasma wavelength (nm)	Carrier density (10^{20} cm^{-3})
0	204±15.4	84.8±4.54	2.17	3.76	4500	1.63
2	223±14.6	89.8±4.32	2.01	4.11	2184	4.7
5	200±14.2	88.4±4.60	1.91	4.20	1725	9.05
7	191±15.6	91.7±4.00	2.04	4.14	1812	8.50
10	235±15.8	90.5±3.87	1.99	4.16	1768	8.4
15	193±16.3	88.0±5.30	2.16	4.09	1851	7.1

$$1/m^*_{VC} = 1/m^*_C + 1/m^*_V, \tag{5}$$

where m^*_C and m^*_V are effective mass of the carriers in the conduction band and valence band, respectively. It should be noted here that at very high carrier densities the electron–electron and electron-impurity scattering could cause a band-gap narrowing.[29,30] Considering both band-gap widening and narrowing effect, the effective band gap should be written by

$$E_g = E_{g0} + \Delta E_g^{\mathrm{B-M}} + \hbar\Sigma, \tag{6}$$

where $\hbar\Sigma$ represents self-energies due to the electron–electron and electron-impurity scattering.[29,30] This effect causes the band-gap narrowing due to the downward shift of the conduction band and upward shift of the valence band.[29,30] However, as shown in Fig. 9(b), the band gap of the ITO films was found to be directly proportional to $N^{2/3}$, showing that the effect of the B–M shift on the band gap dominates over $\hbar\Sigma$.

Sn doping also affects the band gap of the ITO films. Table II shows the effect of Sn doping on the optical properties for the ITO films deposited at 250 °C in 10 mTorr of oxygen gas. The direct band gap was found to initially increase with SnO_2 content up to 5 wt % and slightly decrease up to 15 wt %. This initial increase in band gap is due to an increase in carrier density of the films as a result of Sn doping. This band-gap widening can also be understood by the B–M effect.[26,27] However, above the critical Sn doping, the carrier density decreased with Sn doping because excess Sn causes crystal disorder and the Sn atoms act as carrier traps instead of electron donors. This decrease in carrier density shifted the absorption edge towards lower energies.

The effect of Sn doping was also found to decrease the refractive index, *n*. In Table II, the values of *n* at 550 nm are presented. The refractive index gradually decreases with SnO_2 content up to 5 wt % and then slightly increases up to 15 wt %. This variation of the refractive index with Sn doping can be understood by the relation[31]

$$n^2 = \epsilon_{\mathrm{opt}} - (4\pi N e^2)/(m^* \omega_o^2), \tag{7}$$

where ϵ_{opt} is the high frequency permitivity, *N* is carrier concentration, *e* is the electron charge, m^* is the effective mass of the electron, and ω_o is the frequency of electromagnetic oscillation at which measurements were carried out ($\omega_o = 2\pi c/\lambda$). As the SnO_2 content increased up to 5 wt %, the carrier concentration increased up to 9.05×10^{20} cm^{-3} and thus the value of *n* decreased to 1.91. However, the value of *n* increased again with further increasing SnO_2 content up to 15 wt % due to a decrease in carrier concentration. These results are similar to previous reported values.[31,32] The refractive indices of the films are also affected by the growth temperature. In Table III, it is shown that the value of *n* (at 550 nm of wavelength) decreases from 2.14 to 1.81 with an increase in the substrate deposition temperature from 25 to 300 °C. This decrease in the refractive index can also be explained by an increase in the carrier concentration of the films according to Eq. (7).[31] As the deposition temperature increased up to 300 °C, the carrier density of the films increased (see Fig. 4) and thus, resulted in a reduction of the value of *n*. Shown in Fig. 10 is the dependence of the refrac-

TABLE III. Optical properties of ITO films grown at various temperatures. All films were deposited in 10 mTorr of oxygen using the target with 5 wt % of SnO_2.

Growth temperature (°C)	Film thickness (nm)	Mean transmission (%)	Refractive index at 550 nm	Cutoff wavelength (nm)
25	270±15.5	80.9±8.99	2.14	2475
100	310±14.1	82.4±5.47	2.09	1547
200	290±12.8	84.0±8.99	1.92	1613
300	300±12.0	84.9±8.99	1.81	1713

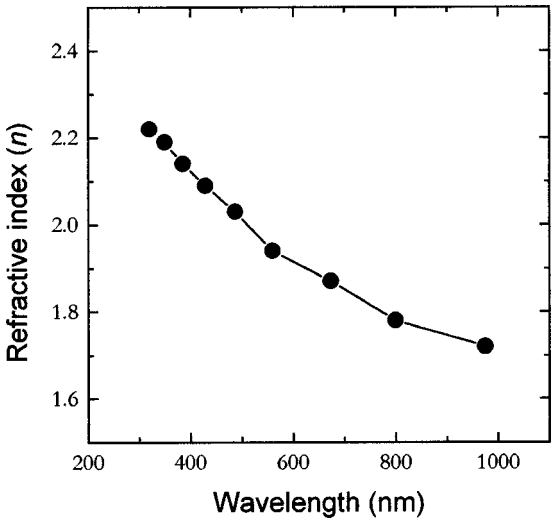

FIG. 10. Variation of refractive index as a function of wavelength for the films deposited at 250 °C and 10 mTorr oxygen.

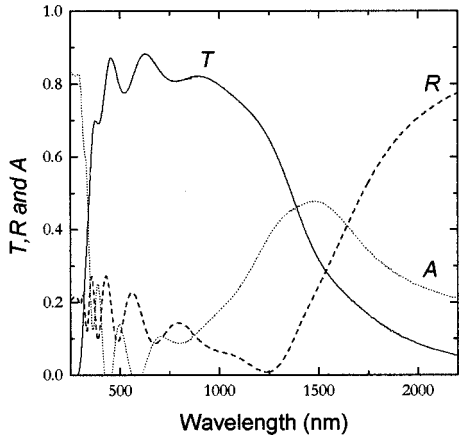

FIG. 11. Typical transmission (T), reflectance (R), and absorption (A) spectra for the ITO film grown at 200 °C and 10 mTorr of oxygen. The film thickness was ~300 nm.

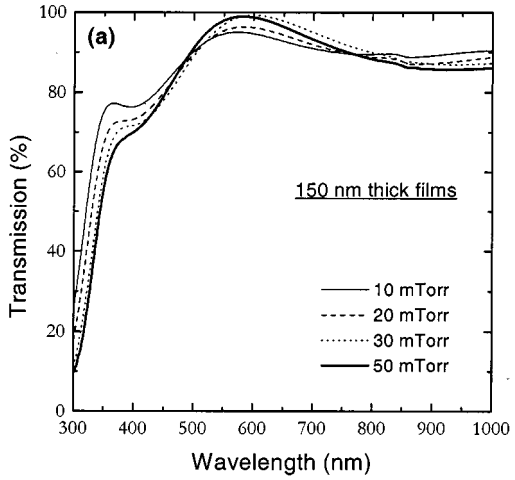

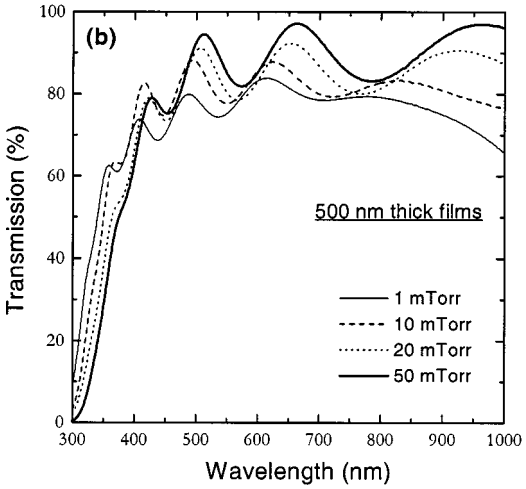

FIG. 12. The effect of oxygen pressure on the optical transmission for the films grown at 300 °C. (a) The thickness of all films was ~150 nm. (b) The film thickness was ~500 nm for all films.

tive index on wavelength for the 300-nm-thick ITO film deposited at 250 °C. An average refractive index of 1.95 ± 0.21 was calculated for the visible range.

In the near-IR region, the interaction of free electrons with incident radiation occurs due to the high number of free electrons in a material. This interaction may lead to polarization of the radiation within the material and thus, affect the relative permittivity ϵ. This optical phenomenon can be understood on the basis of classical Drude's model.[1,22] According to this model,[1,22] ϵ can be written as

$$\epsilon = (n - ik)^2 = \epsilon' + i\epsilon'', \tag{8}$$

$$\epsilon' = n^2 - k^2 = \epsilon_\infty [1 - \omega_p^2/(\omega^2 + \gamma^2)], \tag{9}$$

and

$$\epsilon'' = 2nk = \omega_p^2 \gamma \epsilon_\infty / [\omega(\omega^2 + \gamma^2)]. \tag{10}$$

The plasma resonance frequency ω_p is given by

$$\omega_p^2 = (4\pi N e^2)/(\epsilon_o \epsilon_\infty m_e^*), \tag{11}$$

where ϵ_∞ and ϵ_o represent the dielectric constants of the medium and free space, respectively, m_e^* is the effective mass of the charge carrier, and N is the carrier concentration. γ is equal to $1/\tau$, where τ is the relaxation time, which is assumed to be independent of frequency and is related to mobility as

$$\gamma = 1/\tau = -e/(m_e^* \mu). \tag{12}$$

The cutoff wavelength (or plasma wavelength) λ_p is defined at $T = R$ where the dielectric-like visible transmission equals the metallic-like IR reflectance. The cutoff wavelength λ_p can be obtained from the relation

$$\lambda_p(\mu\text{m}) = 1.24e/(\hbar\omega_p). \tag{13}$$

Table II shows the variation of cutoff wavelength of the films as a function of SnO_2 content (i.e., carrier density). The results can be explained on the basis of Eqs. (11) and (13). The value of λ_p decreased with increasing SnO_2 content, up to 5 wt %, due to the increased carrier density (N) shown in Table II and then increased up to 15 wt % due to a decrease in carrier density. Thus, the value of λ_p can easily be controlled by changing the carrier density through Sn doping: The higher the carrier density, the lower the value of λ_p. This result is in good agreement with the Drude's theory. The substrate deposition temperature also affects the cutoff wavelength λ_p. As shown in Table III, it was observed that the value of λ_p has a minimum of 1547 nm for the film grown at 100 °C. Figure 11 shows the typical transmission (T), reflectance (R), and absorption (A) spectra of the ITO film deposited on glass. The absorption spectra was calculated from the relation: $T + R + A = 1$. The film shows high transparency in the range of 400–1000 nm and high reflectivity in the IR region. The cutoff wavelength of ~1550 nm was observed in this figure.

The optical transmission properties of the films are also affected by oxygen deposition pressure and film thickness as well as substrate deposition temperature. Figure 12(a) shows the effect of oxygen pressure on the optical transmission spectra of the films deposited at 300 °C. The transmission of the 150-nm-thick films was not significantly changed when the oxygen pressure was varied from 10 to 50 mTorr. How-

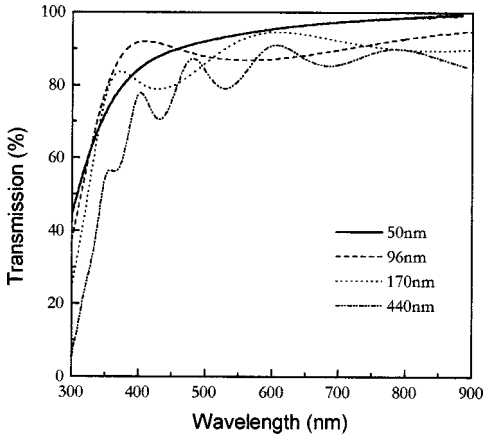

FIG. 13. Effect of film thickness on the optical transmission for the films grown at 300 °C in 10 mTorr of oxygen.

ever, the influence of oxygen pressure on the transmission was distinctly observed as the thickness of the films was increased from 150 to 500 nm. This is well shown in Fig. 12(b), which shows the effect of oxygen pressure on the optical transmission spectra of the 500-nm-thick films deposited at 300 °C. In Fig. 12(b), the optical transmission of the 500-nm-thick films increases with increasing oxygen pressure. This may be due to the improvement of the crystallinity of the ITO films with increasing oxygen pressure, since the grain size of the 500-nm-thick films increased from 15 to 28 nm with an increase in oxygen deposition pressure from 1 to 50 mTorr.

The effect of thickness on the optical transmission of the ITO films is shown in Fig. 13. From Fig. 13, we can see that the optical transmission increases with decreasing film thickness for the films deposited at 300 °C in oxygen pressure of 10 mTorr. According to Eq. (1), the optical transmission (T) exponentially decreases with increasing film thickness (d). However, from Fig. 13, the optical transmission is not exponentially related to the film thickness. This result suggests that the transmission of the ITO films grown by PLD is affected by other physical properties of the films. One possible explanation of this nonexponential relationship between the transmission and the film thickness is an increased grain size with film thickness. According to XRD data, the thicker films usually have larger grain size and the larger grain size results in better transmission. Thus, the larger grain size compensates for the expected exponential decrease in transmission [see Eq. (1)]. In Fig. 13, as the film thickness increases, variations in the transmission are increased due to interference phenomena. The optical transmission properties of the ITO films are also affected by substrate deposition temperature as shown in Table III. Since the grain size of the films also increases with the substrate deposition temperature, the transmission of the films increases with deposition temperature.

C. Structural properties

The crystalline structure of the films was studied by XRD ($\mathrm{Cu}\,K\alpha$, $\lambda = 1.5406$ Å). Figure 3 shows the x-ray diffraction patterns for undoped In_2O_3 and Sn-doped In_2O_3 (ITO) films grown at 250 °C in 10 mTorr of oxygen. Sn-doped In_2O_3 films were always observed to be polycrystalline and showed a similar crystal structure to that of undoped In_2O_3. However, the lattice parameter, calculated from the XRD patterns for undoped In_2O_3 and ITO films, were in the range from 10.122 to 10.238 Å which is normally larger than the JCPDS value[33] of 10.118 Å for the In_2O_3 powder. This increase in lattice constants of the ITO films can be explained by the substitutional incorporation of Sn^{2+} ions into In^{3+} sites and/or the incorporation of Sn ions in the interstitial positions. Since the radius (0.93 Å) of Sn^{2+} ions is larger than that (0.79 Å) of In^{3+}, the substitution of Sn^{2+} for In^{3+} may result in a lattice expansion.[5] This increase in lattice parameters may be also related to oxygen deficiency and strain effect due to thermal expansion coefficient mismatch between the film (7.2×10^{-6} °C)[34] and glass substrate (4.6×10^{-6} °C). Moreover, tin doping changes the grain size of the films. As shown in Fig. 3, the width of the (222) peak is slightly larger as a result of tin doping, indicating that the grain size of the films became smaller. The calculated grain size of the undoped (0 wt %) and tin-doped (10 wt %) films was ~30 and ~20 nm, respectively.

Figure 5 shows XRD patterns of ITO films grown at different substrate deposition temperatures. The films deposited at room temperature (RT) appeared to be amorphous at all oxygen deposition pressures. Despite their amorphous structure, the resistivity of the RT films is low, indicating that in this case the resistivity mechanism is mainly governed by scattering of the electrons by ionized impurities.[23] The films deposited at a temperature of 100 °C showed crystalline structure with a strong (400) diffraction peak, indicating a preferred orientation along the [100] direction. As the deposition temperature was further increased up to 300 °C, the preferred orientation peak of the films changed to (222). By fitting of the diffraction peaks, the grain size and lattice parameter of the films were calculated. As shown in Table I, as the deposition temperature increases from 100 to 300 °C, the grain size of the films increases from ~10 to ~20 nm and the lattice parameter of the ITO films increases from 10.2217 ± 0.0072 to 10.2381 ± 0.0082 Å.

The crystalline structure of the films was also affected by oxygen pressure during deposition. Figure 7 shows the XRD patterns of the films deposited at 300 °C in different oxygen pressures. From the patterns, we can see that the films have a ⟨111⟩ preferred orientation. As the oxygen pressure increases from 1 to 100 mTorr, the intensity of the (222) peak increases, indicating that the films are more crystalline and maintains a ⟨111⟩ preferred orientation. Moreover, when the oxygen pressure increases, the linewidth of the (222) reflection decreases, indicating that the grain size of the film is increasing. Even though the grain size of the films increases with oxygen pressure, the resistivity of these films increases with oxygen pressure. This indicates that the contribution of grain boundary scattering is not the dominant scattering mechanism in these films. This can also be understood from the mobility data shown in Fig. 6. The mobility of the carriers in the films decreases as the oxygen pressure increases. This suggests that the dominant scattering mechanism in these films is ionized impurity scattering because the

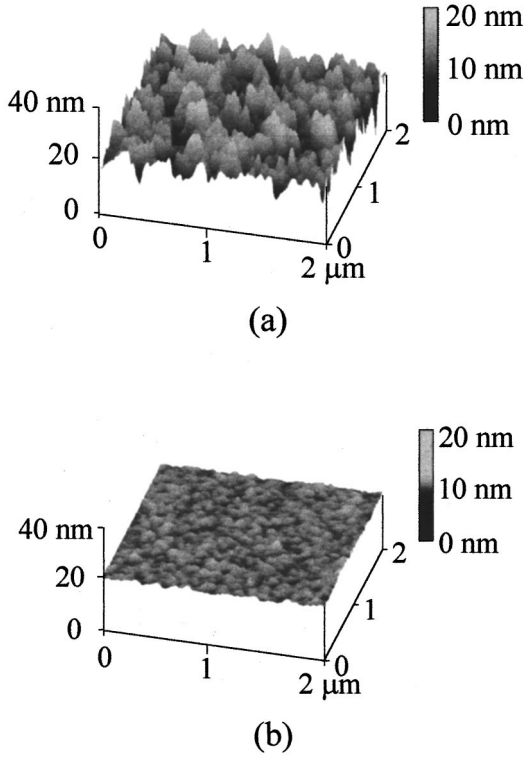

FIG. 14. AFM images (2 μm×2 μm) of the ITO films grown on glass substrates by (a) sputtering (supplied by Planar America) and (b) PLD. Note that the scale in the *z* direction (20 nm/div.) is greatly expanded with respect to the scales in the *x* and *y* directions (1.0 μm/div.) and therefore, in fact, the crystallites are flat and broad in the lateral direction.

oxygen vacancies behave as ionized impurity scattering centers in addition to the tin dopants. However, as oxygen pressure increases, the carrier concentration decreases due to the fewer oxygen vacancies in the film and consequently conductivity decreases (see Fig. 6).

D. Surface morphology

Since the organic thin films in OLEDs are directly deposited on the ITO anode, the surface properties of the ITO will affect the characteristics of the device. Figure 14 shows two AFM images (2 μm×2 μm) of ITO films deposited by sputtering (supplied by Planar America) and PLD. The thickness of both films is about 180 nm. Prior to AFM measurements, the films were washed with methanol and blown dry with nitrogen gas. The root-mean-square (rms) surface roughness for the ITO film deposited by PLD at a substrate temperature of 300 °C and oxygen pressure of 10 mTorr is ~4.4 Å compared to a value of ~12.5 Å for the bare glass substrate. However, the rms surface roughness of the film deposited by sputtering is ~39 Å compared to a value of 16.2 Å for the bare glass substrate. This indicates that these PLD ITO films show lower surface roughness than that of sputtered ITO films. The grain sizes of the film shown in Fig. 14(b) were observed to be 20–40 nm.

E. Figure of merit

The simultaneous achievement of maximum optical transmission and electrical conductivity is not possible since these two properties are inversely related. Therefore, a figure of merit has been developed to compare transparent conducting oxide (TCO) films like ITO. There have been several reports on the definition of a suitable figure of merit. One of the common definitions was proposed by Fraser and Cook[35] who defined $F_{TC}=T/R_s$, where T is the optical transmission and R_s the electrical sheet resistance. However, on the basis of this figure of merit F_{TC}, the maximum F_{TC} occurs at 37% of optical transmission and thus the electrical sheet resistance was over emphasized in its relative importance to the optical transmission for films. An optimal consideration between electrical sheet resistance and optical transmission was achieved by Haacke[36] who defined the figure of merit as $\phi_{TC}=T^{10}/R_s$. On this basis, ϕ_{TC} has the maximum value at 90% of optical transmission. In Table IV, the values for F_{TC} and ϕ_{TC} for the ITO films prepared in this work are compared with those of the films prepared by other techniques reported in the literature. Table IV shows that the ITO films can be made by PLD at low processing temperatures with comparable F_{TC} values to other procedures. From Table IV, it can also be seen that PLD can be used to grow ITO films with comparable electrical and optical properties to those of commercial films.

F. Device performance with PLD ITO anode

Figure 15 shows the schematic structure of an OLED used in this research. The device structure is made of a hole transport layer [(HTL), ~500 Å thick] of *N*,*N*′-diphenyl-*N*,*N*-bis (3-methylphenyl)1,1′-diphenyl-4,4′diamine (TPD), and an electron transport/emitting layer [(ETL/EML), ~700 Å thick] of tris (4-methyl-8-hydroxyquinolinolato) aluminum

TABLE IV. Comparison of values of figure-of-merit ϕ_{TC} and F_{TC} for ITO films prepared by different techniques.

Process	Substrate temperature (°C)	Film thickness (nm)	Sheet resistance R_s(Ω/sq.)	Transmission (λ=400–700 nm) (%)	Figure of merit $F_{TC}(\times 10^{-3}\ \Omega^{-1})$	Figure of merit $\phi_{TC}(\times 10^{-3}\ \Omega^{-1})$
Present work	25	150	27	85	31	7.3
Sputtering (Ref. 5)	130	80	62	85	14	3.2
Present work	300	180	11	92	84	39.5
CVD (Ref. 3)	400	430	6.74	80	118	15.9
Spray (Ref. 7)	420	350	9.34	85	91	21
Commercial	Proprietary					
		180	12	90	90	34.9
(sputtering)	(>25)					

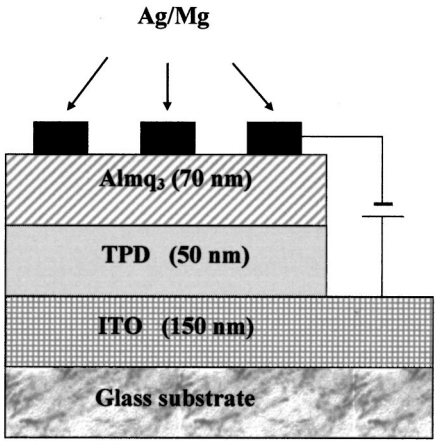

FIG. 15. Schematic structure of an organic light-emitting device (OLED) with an ITO anode deposited by PLD. ITO film, grown at room temperature in oxygen pressure of 10 mTorr, was used in this device.

(III) ($Almq_3$). The cathode contact deposited on top of the ETL is an alloy of Mg:Ag (ratio=12:1 and a thickness of 1000 Å). Details on the fabrication of these devices are described elsewhere.[37–39] The active area for the device is $\sim 2\times 2$ mm^2. The current–voltage–luminance (I–V–L) data were taken (in N_2 atmosphere) using a Keithley current–voltage source and a luminance meter (Minolta LS-110). Figure 16(a) shows the current–voltage–luminance output (I–V–L) characteristics of an OLED with an ITO anode grown on glass by PLD at room temperature. The I–V and L–V curves show a typical diode behavior, with current and power output observed only in the forward bias. As shown in Fig. 16(b), furthermore, the data for L and I superimpose quite well, in agreement with what has been reported using commercial ITO. The device external quantum efficiency measured for such a heterostructure device was $\eta_{ext} \cong 1.5\%$ at 100 A/m^2. This value is comparable to those reported recently ($\eta_{ext} \cong 1.5\%-2.5\%$) using commercial ITO from different sources as the anode contact.[37–39] The above value for η_{ext} indicates that ITO films, grown by PLD at RT, are working well.

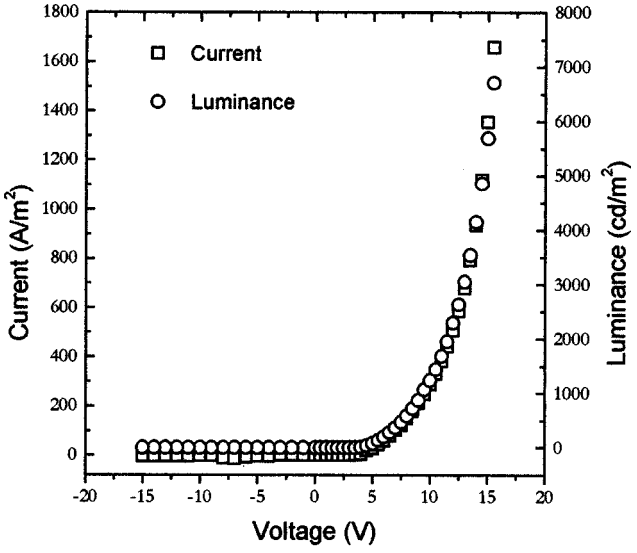

(a)

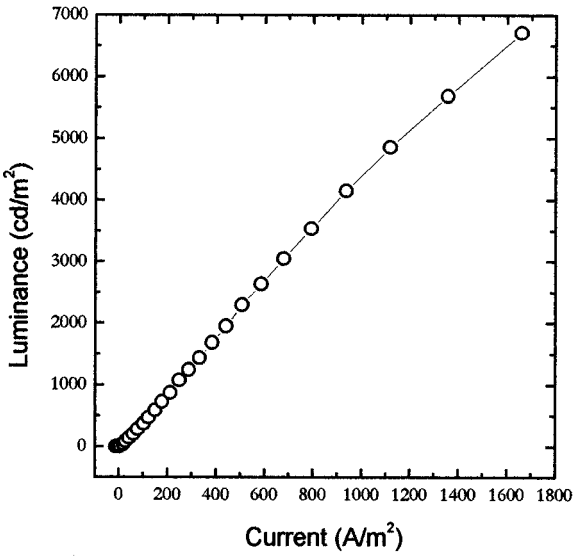

(b)

FIG. 16. (a) Current–voltage–luminance (I–V–L) and (b) luminance–current (L–I) characteristics of a heterostructure device with a PLD ITO film as the hole injecting layer to TPD layer. ITO film, grown at room temperature in oxygen pressure of 10 mTorr, was used in this device.

IV. SUMMARY

High-quality ITO films have been deposited on glass substrates by PLD. The electrical, optical and structural properties of the ITO films have been investigated as a function of target composition, substrate deposition temperature, oxygen background gas pressure, and film thickness. All of the ITO films grown by PLD were found to be n-type semiconductors. A SnO_2 content of 5 wt% in the target was observed to produce films with a minimum resistivity. However, for films deposited from a target with greater than 5 wt% of SnO_2, an increase in the resistivity was observed. It is possible that excess Sn atoms may form clusters and distort the lattice as well as produce additional scattering centers. Increasing the substrate deposition temperature created more Sn donors and oxygen vacancies and resulted in a higher electron concentration, and thus increased conductivity of the films. A reduced oxygen pressure from 50 to 10 mTorr resulted in more oxygen vacancies and increased the conductivity of the films. However, a further decrease in oxygen pressure below 10 mTorr caused lattice structural disorder and hence decreased conductivity. As the thickness of the ITO films was increased, the films deposited at 300 °C become more crystalline and had larger grain sizes, which resulted in an increase of their conductivity.

The optical properties such as band gap, refractive index, plasma wavelength, optical transmission, and reflectance for the ITO films were strongly affected by tin-dopant concentration and deposition conditions. The band-gap widened with an increase in carrier concentration. This band-gap wid-

ening is well explained by the B–M shift theory.[26,27] A reduction of the refractive index for ITO films due to increased electron density in the films was observed by increasing Sn dopants in the targets and/or increasing deposition temperature. The plasma wavelength of the ITO films was controlled by changing the doping level in the targets or changing deposition temperature. The optical transmission of the films was also controlled by target SnO_2 content, substrate deposition temperature, oxygen deposition pressure, and film thickness. At the conditions optimized for maximum transmission and minimum resistivity films (target composition with 5 wt% SnO_2, 250 °C, 10 mTorr, and 190 nm), the optical transmission of the ITO films in the visible range was 91.7%. For a 150-nm-thick film grown at room temperature in oxygen pressure of 10 mTorr, the resistivity was 4×10^{-4} Ω cm and the average transmission in the visible range of 85% was observed. For 170-nm-thick films deposited at 300 °C in 10 mTorr of oxygen, the resistivity was 2×10^{-4} Ω cm and the average transmission in the visible range was 91%.

ITO films deposited by PLD had surface roughness approximately 1 order of magnitude smaller than commercial films grown by sputtering. We used these ITO films as the anode contact in OLEDs and studied the device performance. Electroluminescence (EL) efficiencies comparable to those reported with commercial ITO films have been observed for heterostructure devices made of TPD/$Almq_3$. This indicates the promise of the present approach for making good quality ITO films at room temperature with a potential application in OLEDs.

ACKNOWLEDGMENTS

This work was financially supported by Office of Naval Research. $Almq_3$ was kindly supplied by Professor Junji Kido of Yamagata University, Japan. We would like to thank Dr. Eric Jackson for his help relating Hall effect measurements.

[1] H. L. Hartnagel, A. L. Dawar, A. K. Jain, and C. Jagadish, *Semiconducting Transparent Thin Films* (Institute of Physics, Bristol, 1995).
[2] H. Kim, A. Piqué, J. S. Horwitz, H. Mattoussi, H. Murata, Z. H. Kafafi, and D. B. Chrisey, Appl. Phys. Lett. **74**, 3444 (1999).
[3] C. W. Tang and S. A. Van Slyke, Appl. Phys. Lett. **51**, 913 (1987).
[4] T. Maruyama and K. Fukui, Thin Solid Films **203**, 297 (1991).
[5] W.-F. Wu, B.-S. Chiou, and S.-T. Hsieh, Semicond. Sci. Technol. **9**, 1242 (1994).
[6] M. Buchanan, J. B. Webb, and D. F. Williams, Appl. Phys. Lett. **37**, 213 (1980).
[7] P. Nath, R. F. Bunshah, B. M. Basol, and O. M. Staffsud, Thin Solid Films **72**, 463 (1980).
[8] V. Vasu and A. Subrahmanyam, Thin Solid Films **193/194**, 696 (1990).
[9] J. P. Zheng and H. S. Kwok, Appl. Phys. Lett. **63**, 1 (1993).
[10] C. Coutal, A. Azema, and J.-C. Roustan, Thin Solid Films **288**, 248 (1996).
[11] F. Hanus, A. Jadin, and L. D. Laude, Appl. Surf. Sci. **96–98**, 807 (1996).
[12] D. B. Chrisey and G. K. Hubler, *Pulsed Laser Deposition of Thin Films* (Wiley, New York, 1994).
[13] D. K. Schroder, *Semiconductor Material and Device Characterization* (Wiley, New York, 1990).
[14] J. Kane, H. P. Schweizer, and W. Kern, J. Electrochem. Soc. **127**, 1592 (1980).
[15] B. D. Cullity, *Elements of X-ray Diffraction*, 2nd ed. (Addison–Wesley, Reading, MA, 1978).
[16] J. C. Manifacier, Thin Solid Films **90**, 297 (1982).
[17] S. A. Agnihotry, K. K. Saini, T. K. Saxena, K. C. Nagpal, and S. Chandra, J. Phys. D **18**, 2087 (1985).
[18] M. Mizuhashi, Thin Solid Films **70**, 91 (1980).
[19] H. Köstlin, R. Jost, and W. Lems, Phys. Status Solidi A **29**, 87 (1975).
[20] S. Noguchi and H. Sakata, J. Phys. D: Appl. Phys. **114**, 1523 (1981).
[21] J. C. Manifacier, L. Szepessy, J. F. Bresse, M. Perotin, and R. Stuck, Mater. Res. Bull. **14**, 109 (1979).
[22] J. L. Vosssen, Phys. Thin Films **9**, 1 (1977).
[23] R. Clanget, Appl. Phys. **2**, 247 (1973).
[24] T. Karasawa and Y. Miyata, Thin Solid Films **233**, 135 (1993).
[25] J. Tauc, R. Grigorovici, and A. Vancu, Phys. Status Solidi **15**, 627 (1966).
[26] E. Burstein, Phys. Rev. **93**, 632 (1954).
[27] T. S. Moss, Proc. Phys. Soc. London, Sect. B **67**, 775 (1954).
[28] I. Hamberg and C. G. Graqvist, J. Appl. Phys. **60**, R123 (1986).
[29] C. H. L. Weijtens and P. A. C. van Loon, Thin Solid Films **196**, 1 (1991).
[30] L. Gupta, A. Mansingh, and P. K. Srivastava, Appl. Surf. Sci. **33/34**, 898 (1988).
[31] R. T. Chen and D. Robinson, Appl. Phys. Lett. **60**, 1541 (1992).
[32] Y. Ohhata, F. Shiniki, and S. Yoshida, Thin Solid Films **59**, 255 (1979).
[33] JCPDS Card No. 06-0416.
[34] W.-F. Wu and B.-S. Chiou, Thin Solid Films **293**, 244 (1997).
[35] D. B. Fraser and H. D. Cook, J. Electrochem. Soc. **119**, 1368 (1972).
[36] G. Haacke, J. Appl. Phys. **47**, 4086 (1976).
[37] J. Kido and Y. Iizumi, Chem. Lett. **10**, 963 (1997).
[38] J. Kido and Y. Iizumi, Appl. Phys. Lett. **73**, 2721 (1998).
[39] H. Murata, C. D. Merritt, H. Mattoussi, and Z. H. Kafafi, Proc. SPIE **3476**, 88 (1998).